# Computational Study of the Supersonic Molecular Beam Injection in Thailand Tokamak-1 based on the 2D Fluid Model

Kitti RONGPUIT[1)], Apiwat WISITSORASAK[1,2)] and Jiraporn PROMPING[3)]

[1)]*Theoretical and Computational Physics Group, Department of Physics, Faculty of Science, King Mongkut's University of Technology Thonburi, Bangkok, Thailand*

[2)]*Center of Excellence in Theoretical and Computational Science, King Mongkut's University of Technology Thonburi, Bangkok, Thailand*

[3)]*Thailand Institute of Nuclear Technology (Public Organization), Nakhon Nayok, Thailand*

(Received 27 February 2023 / Accepted 24 November 2023)

The successful operation of a tokamak requires effective and appropriate methods of plasma fueling. In the development plan for Thailand Tokamak-1 (TT-1), the use of supersonic molecular beam injection (SMBI) has been proposed as a method that can more effectively and deeply deliver fueling gas compared to the gas puffing method. In this study, we used 2D fluid simulation to investigate the impact of SMBI on plasma transport in TT-1. Our model incorporated the continuity equations, energy balance equations, momentum equation, continuity of fuel equations, and momentum equation of fuel. BOUT++ is then used to solve these equations by a finite difference method with the field-aligned coordinates in the edge region of the tokamak. Our simulation results showed that when hydrogen fuel gas is injected into the plasma via SMBI from the low-field side at the speed in the range of 600 - 1200 m/s, the electron density in the edge region locally increases due to dissociation and ionization in the region where the fuel gas meets the plasma. This subsequently leads to a decrease in the ion and electron temperatures. The increased density then spreads throughout the plasma volume within approximately 10 ms. Increasing the injection speed leads to a deeper penetration length for the fuel deposition.



Keywords: BOUT++ code, fusion energy, supersonic molecular beam injection, Thailand Tokamak-1

DOI: 10.1585/pfr.19.1403002

## 1. Introduction

In order to achieve the necessary fusion power performance at high density in next-generation devices like ITER, it is essential to have plasma fueling with improved efficiency and deeper injection. The supersonic molecular beam injection (SMBI) has been recognized as a highly effective method for fueling plasma, and has been demonstrated through experimentations and computational analysis to be more efficient than the gas puffing (GP) method in terms of delivering fuel deeper into the plasma. The SMBI method can penetrate to a similar depth as pellet injection (PI) for fuel deposition, but it is more cost-effective than the PI. SMBI has been implemented in various tokamak devices, including HL-2A [1], J-TEXT [2], KSTAR [3], JT-60U [4], and EAST [5, 6].

Thailand Tokamak-1 (TT-1), the first small research tokamak in Thailand, is operated by the Thailand Institute of Nuclear Technology in Nakhonnayok province. It has a major radius of 0.65 m, a minor radius of 0.20 m, a toroidal magnetic field ranging from 1.0 to 1.5 T, and a plasma current ranging from 60 to 150 kA [7]. Poloidal limiters are also installed in this device and allows the plasma with a circular shape. In the initial phase of the operation, TT-1 will run the hydrogen plasma operation and can only be fueled by the GP method. However, the SMBI technique will eventually be designed, built, installed, and used in the TT-1 tokamak. The primary objective of this work is to computationally investigate the transport dynamics of the TT-1 plasma while fueling it using the SMBI method. While the TT-1 successfully achieved the first hydrogen plasma operation in early 2023, the device has not yet installed the SMBI system. The SMBI system of the TT-1 is expected to be operational within 1 to 2 years.

Numerous experimental studies have been conducted to understand underlying physics mechanism and improve the penetration depth and fueling efficiency of the SMBI technique. In addition, this method has been shown to be an effective tool for controlling plasma density [8], improving plasma confinement [9], and mitigating edge localized modes (ELM) [10].

In order to computationally investigate the dynamics of plasma and the fuel during the SMBI fueling, it is important to understand its transport dynamics. The fuel gas of SMBI is launched into the plasma at a high speed ranging from 500 to 1200 m/s, but the gas is nearly at room temperature. In contrast to the gas puff (GP) method, the transport of SMBI is primarily driven by the convection process rather than diffusion. Several codes, such as B2-EIRENE

*author's e-mail: apiwat.wis@kmutt.ac.th*

[11], EPIC [12], UEDGE [13, 14], and TPSMBI [15], have been developed based on the classical fluid model of SMBI and are able to simulate transport in a toroidal geometry. For studying the SMBI in TT-1, a simple one-dimension fluid model was developed [16]. The model includes transport equations of three particle species (plasma, atom and molecules of fuel gas) such as plasma, heat and momentum transport equations, molecule density and radial momentum transport equations, and atom density transport equation. This model only considers the transport along the radial direction, while injection of the fuel gas breaks the poloidal symmetry. The present work therefore developes the 2D fluid simulation for investing SMBI in the TT-1 plasma.

This paper is organized as follows. Section 2 presents the physical model and numerical method that is used in this work. Then we discuss the simulation results in Sec. 3. Section 4 summarizes this study and future prospective about the work is discussed.

## 2. Methodology

When fuel gas is introduced into a tokamak plasma by SMBI, a variety of collision reactions occur between particles of molecules, atoms, and the plasma. These reactions include molecular dissociation, atom ionization, charge exchange, and electron-ion recombination, among others. To simplify the analysis, we assume that the fuel gas is successfully delivered to the edge of the plasma. In order to model the transport physics of the fueling process, four particle species are considered: hydrogen molecules (fuel gas), hydrogen atoms, hydrogen ions, and electrons. The model used in this work is based on the Braginskii equations and consists of six equations [17, 18]. The equations are derived to incorporate the basic transport physics during the fueling process and provide a comprehensive understanding of the underlying processes.

This research utilizes the finite difference method and the BOUT++ code framework to solve the transport equations [19–21]. This approach is particularly advantageous as it allows for the solution of the equations in a field-aligned coordinate system, which are closely related to the standard flux coordinates and are widely used in tokamak turbulence simulations [22, 23]. The selection of this method and framework ensures an accurate and efficient solution of the transport equations. In this coordinate system, the radial-like coordinate is represented by $x$, and $x =$ constant corresponds to a fixed flux surface. The poloidal-like coordinate is represented by $y$, and $z$ refers to the toroidal-like coordinate in the bi-normal direction.

In the current study, the charge quasi-neutrality condition of the plasma is applied, i.e. $n_i \approx n_e$. The continuity of the plasma density is expressed as follows:

$$\frac{\partial n_i}{\partial t} + \nabla_{\parallel}(V_{\parallel,i} n_i) - D^c_{\perp,i}\nabla^2_{\perp}(n_i) \quad = \quad S^p_i - S^p_{\rm rec}, \quad (1)$$

where $n_i$, $V_{\parallel,i}$, $D^c_{\perp}$, $S^p_i$ and $S^p_{\rm rec}$ are plasma density, the ion parallel velocity, perpendicular diffusion coefficient of density, the atom ionization rate, the atom ion and electron recombination rates, respectively. The parallel ($\parallel$) and perpendicular ($\perp$) subscripts refer to the parallel and perpendicular directions to the magnetic field lines.

The equation for the electron temperature is formulated as follows:

$$\begin{aligned}\frac{\partial T_e}{\partial t} &+ \frac{2}{3n_i}\nabla_{\parallel}(\kappa^c_{\parallel,e} T_e) - \frac{2}{3}\chi^c_{\perp,e}\nabla^2_{\perp}(T_e) \\ &= \nu_{\rm rec} W_{\rm rec} - \nu_I(T_e + \frac{2}{3}W_I) \\ &\quad -\frac{2}{3}\nu_{\rm diss}(W_{\rm diss} + W_{\rm bind}) - \frac{2m_e}{M_i}\frac{T_e - T_i}{\tau_e}, \end{aligned} \quad (2)$$

where $T_e$, $\kappa^c_{\parallel}$ and $\chi^c_{\perp,e}$ are the electron temperature, parallel thermal conductivity coefficients of electron and diffusion coefficient of electron temperature, respectively. Reaction rates $\nu_I$, $\nu_{\rm rec}$ and $\nu_{\rm diss}$ are referred to the atom ionization, plasma recombination, and molecular dissociation rates, respectively. While $W_I$ and $W_{\rm diss}$ are electron energy lost due to the ionization and dissociation, and $W_{\rm bind}$ is the binding energy between the two hydrogen atoms in a molecule. The equation for the ion temperature is written as:

$$\begin{aligned}\frac{\partial T_i}{\partial t} &+ V_{\parallel,i}\nabla_{\parallel,i}T_i + \frac{2}{3}T_i\nabla_{\parallel,i}V_{\parallel,i} - \frac{2}{3n_i}\nabla_{\parallel}(\kappa^c_{\parallel,i}\nabla_{\parallel}T_i) \\ &-\frac{2}{3}\chi^c_{\perp,i}\nabla^2_{\perp}T_i = (\nu_{\rm rec} - \nu_I)T_i \\ &-\frac{2m_e}{M_i}\frac{T_e - T_i}{\tau_e}, \end{aligned} \quad (3)$$

where $T_i$ and $\kappa^c_{\parallel,i}$ are the ion temperature and parallel thermal conductivity coefficients of ion respectively. $\chi^c_{\perp,i}$ is perpendicular diffusion coefficient of ion density. The values of the transport coefficients are generally non-uniform and depend on several factors [24]. For simplicity, this work, however, assumes uniform values as follows: $D^c_{\perp} = 1.0\,m^2/s$, $\chi^c_{\perp} = 2.0\,m^2/s$ and $\chi^c_{\perp,e} = 1.0\,m^2/s$.

The parallel velocity of ions ($V_{\parallel,i}$) can be determined using the parallel momentum equation

$$\begin{aligned}\frac{\partial V_{\parallel,i}}{\partial t} &+ V_{\parallel,i}\nabla_{\parallel}V_{\parallel,i} - \frac{4}{3n_iM_i}\nabla_{\parallel}(\eta^0_i\nabla_{\parallel}V_{\parallel,i}) \\ &= -\frac{\nabla_{\parallel}P}{n_iM_i} - (\nu_{CX} + \nu_I)V_{\parallel,i}, \end{aligned} \quad (4)$$

where $\nu_{\rm cx}$ and $\nu_I$ are the ion-atom charge exchange rate and atom ionization rate respectively. $\eta^0_i$ is the ion viscosity and equals $\eta^0_i = 0.96 n_i k T_i \tau_i$.

The following are the definitions of quantities associated with the sources and rates resulting from particle collision reactions. These definitions are essential in order to fully comprehend the underlying processes taking place in the collisions of the tokamak plasma and fuel gas.

$$\begin{aligned} S^p_{\rm rec} &= n_e\nu_{\rm rec}, & S^p_I &= n_e\nu_I = n_a\nu^a_I, \\ S^p_{CX} &= n_{\rm a}\nu^a_{\rm cx}, & S^p_{\rm diss} &= n_e\nu_{\rm diss} = n_m\nu^m_{\rm diss}, \\ \nu_{\rm diss} &= n_m\langle\sigma_{\rm diss}V_{\rm th,e}\rangle, & \nu_{\rm cx} &= n_a\langle\sigma_{CX}V_{th,i}\rangle, \end{aligned}$$

$$\nu^a_{\rm cx} = n_i\langle\sigma_{\rm cx}V_{\rm th,i}\rangle, \qquad \nu^a_{\rm I} = n_e\langle\sigma_{\rm I}V_{\rm th,e}\rangle,$$
$$\nu_{\rm rec} = n_e\langle\sigma_{\rm rec}V_{\rm th,e}\rangle, \qquad \nu^m_{\rm diss} = n_e\langle\sigma_{\rm diss}V_{\rm th,e}\rangle.$$

In the transport of neutral gas due to SMBI, we assume that the gas molecule is conveyed by a speed of $V_{\rm xm}$ in the radial direction as it enters the confined plasma volume. The gas molecule then undergoes dissociation and ionization processes. The continuity equations for fuel molecules and atoms can be written as follows:

$$\frac{\partial n_m}{\partial t} + \nabla_x(V_{\rm xm}n_m) = -S^p_{\rm diss}, \tag{5}$$

$$\frac{\partial n_a}{\partial t} - \nabla_\parallel(D^c_{\parallel,a}\nabla_\parallel n_a) - D^c_{\perp,a}\nabla^2_\perp n_a = -S^p_I + S^p_{\rm rec} + 2S^p_{\rm diss}, \tag{6}$$

where $D^c_{\perp,a}$ and $D^c_{\parallel,a}$ are perpendicular and parallel diffusion coefficients of the fuel atoms, and have the form: $D^c_{\perp,a} = D^c_{\parallel,a} = \dfrac{T_a}{M_a\nu^a_{\rm cx}}$, where $M_a$ is the mass of hydrogen atom, where $S^p_{\rm diss} = n_e\nu_{\rm diss} = n_m\nu^m_{\rm diss}$ is molecular dissociation source rate. The hydrogen plasma is also assumed in this work.

The following is the equation for the momentum of the molecular density, which describes the motion of the molecular density in the plasma:

$$\frac{\partial V_{\rm xm}}{\partial t} + V_{\rm xm}\nabla_x V_{\rm xm} = -\frac{\nabla_x P_m}{n_m M_m}, \tag{7}$$

where the molecular pressure $P_m = kn_mT_m$, and the molecule is assumed for having the room temperature ($T_m = 300$ K).

The reaction rate coefficients ($\nu$) in the reaction rates are a function of the ion and electron temperatures and can be accurately represented by empirical formulas [25]. These formulas, which are derived from experimental data, provide a reliable way to calculate the reaction rates in the tokamak plasma and are given as follows (provided in the unit of cm$^3$ s$^{-1}$) [15].

$$\langle\sigma_{\rm I}V_{\rm th,e}\rangle = 3\times10^{-8}\times\frac{(0.1T_e)^2}{3+(0.1T_e)^2},$$
$$\langle\sigma_{\rm cx}V_{\rm th,i}\rangle = 1.7\times10^{-8} + 1.9\times10^{-8}\times\frac{(1.5T_i)^{1/3}-(15)^{1/3}}{(150T_i)^{1/3}-(15)^{1/3}},$$
$$\langle\sigma_{\rm diss}V_{\rm th,e}\rangle = 3\times10^{-8}\times\frac{(0.1T_e)^2}{3+(0.1T_e)^2},$$

where $T_e$ and $T_i$ in the above formulas are given in the unit of eV. Note that the parallel thermal conductivities of ions and electrons are expressed as $\kappa^c_{\parallel,i} = 3.9n_ikT_i\tau_i/M_i$ and $\kappa^c_{\parallel,e} = 3.2n_ekT_e\tau_i/m_e$.

In this study, the focus is on the transport of the SMBI in TT-1. The magnetic flux surface in TT-1 has a nearly circular geometry, with a limiter that extends from the wall into the plasma volume, as depicted in Fig. 1 (a). The blue dashed line in the figure represents the separatrix, which separates the confined plasma from the open field lines. The innermost flux surface has radial boundary conditions, with fixed-gradients applied to the ion density ($n_i$) and the ion and electron temperatures ($T_i$, $T_e$) as determined from experiments or simulations. These conditions represent continuous inflows of particles and heat from the core. All other variables are subjected to Neumann boundary conditions at this boundary.

At the outermost magnetic flux surface, fixed values are applied as boundary conditions for the ion density ($n_i$), ion temperature ($T_i$), and electron temperature ($T_e$) using Dirichlet boundary conditions. For the transport of the fuel gas, it is launched at the midplane on the low-field side and the molecular density ($n_m$) and radial velocity ($V_{xm}$) at this surface are determined through a Gaussian distribution over the poloidal angle, specified by Dirichlet boundary

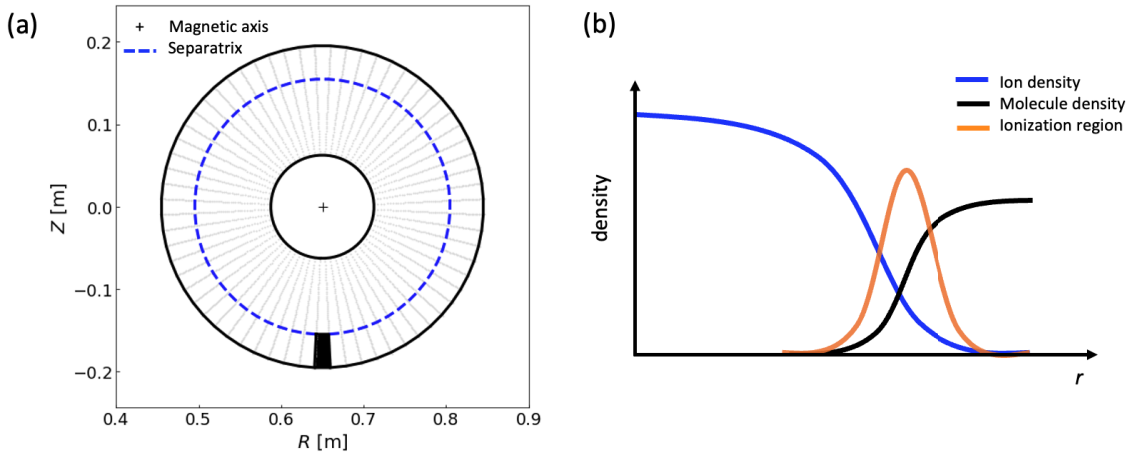


Fig. 1 (a) The cross-section of the magnetic flux surface mesh of TT-1 used in the study is presented. The computational domain encompasses the region between $\psi = 0.4$ and 1.2. The separatrix is indicated by the blue dashed line, while the limiter is depicted in black at the bottom. (b) Simple diagram representing typical profiles of the electron density ($n_i$), the fuel gas molecule ($n_m$), and the ionization region.

conditions:

$$n_{\mathrm{m,edge}} = n_{\mathrm{m0}}\, e^{-(\theta-\theta_0)^2/\sigma_\theta^2}, \quad (8)$$

$$V_{\mathrm{xm,edge}} = V_{\mathrm{xm0}}\, e^{-(\theta-\theta_0)^2/\sigma_\theta^2}, \quad (9)$$

where $\theta_0$ denotes the central angle along the poloidal plane of the injection path, $\sigma$ specifies the width of the SMBI in the poloidal direction, and $n_{\mathrm{m0}}, V_{\mathrm{xm0}}$ are constants that set the values of the molecule density and radial velocity, respectively, at the outermost flux surface. In order to simulate the sequence of gas injection, we apply the boundary values of $n_{m0}$ and $V_{xm0}$ as follows: for the events before and after the injection, $n_{m0}$ and $V_{xm0}$ are set to zero. When the fuel is introduced into the plasma, $n_{m0}$ and $V_{xm0}$ take on non-zero values. Here, we assume that $n_{m0}$ is equal to $2 \times 10^{17}$ m$^{-3}$, whose value strongly depends on the beam pressure. The values of $V_{xm0}$ are within the range of $-500$ m/s to $-1200$ m/s, with negative values indicating the inward direction.

# 3. Simulation Results and Discussion

BOUT++ is a modular, object-oriented framework that is utilized to study the physics of the boundary plasma [19]. It covers the separatrix and includes boundary conditions for both closed magnetic flux surfaces and open field lines. In this study, the 4th order central differencing method is used for first and second order derivatives, and the third-order WENO (weighted essentially non-oscillatory) scheme is applied for convective terms [26]. To accurately solve the partial differential equations present in the BOUT++ framework, a method-of-lines approach is employed in conjunction with an implicit backward differencing scheme. The implicit backward differencing scheme utilizes the Newton-Krylov solver PVODE to provide a robust and efficient solution to the equations. This approach ensures that the solutions obtained are accurate and computationally efficient.

This study aims to simulate the plasma response during the SMBI in the Thailand Tokamak-1 (TT-1) device. It is essential to note that TT-1 has a major radius of 0.65 m, a minor radius of 0.20 m, a plasma current of approximately 100 kA, and a toroidal magnetic field at the magnetic axis assumed to be 1.0 T. The device is equipped with a limiter that extends into the plasma volume and the plasma is assumed to have a nearly circular shape. In our simulations, the resolutions in the $x$ and $y$ directions are set at 64×64 grids. The cross-section toroidal equilibrium used in this work is based on the TT-1 configuration computed by the FreeGS code. The radial domain of the normalized magnetic flux $\psi$ is defined as $\psi = 0.4$ - $1.2$, with $\psi = 1.0$ located at the separatrix, which is defined as the tip of the limiter, see Fig. 1. Our simulations consider the scenario where hydrogen gas is injected into the tokamak via SMBI, and it is assumed that this injection takes place at the midplane of the tokamak on the low-field side (LFS). The initial profiles for the plasma density and temperatures are obtained from a CRONOS integrated predictive simulation that numerically investigates the Ohmic phase of the TT-1 plasma [27]. The electron density near the magnetic axis is estimated to be approximately $2 \times 10^{19}$ m$^{-3}$, while the temperatures of the electrons and ions at the core are approximately 2500 eV and 750 eV, respectively.

We first present the results of simulations that investigate the SMBI at a constant injection velocity of $-500$ m/s in Sec. 3.1. These results provide a baseline for understanding the behavior of the plasma under these conditions. We then proceed to explore multiple cases in which the injection speed is varied between 600 - 1200 m/s in Sec. 3.2. This allows us to understand the effect of varying the injection speed on the plasma response and behavior during SMBI.

## 3.1 Simulations with a constant injection speed

TT-1 is a small tokamak that operates with hydrogen plasma. In this work, it is assumed that SMBI is delivered into the device from the low-field side (LFS). The simulation further assumes that hydrogen gas is injected with a speed of 500 m/s at the midplane for a period of 1.00 ms (between $t$ = 1.00 - 2.00 ms). After $t$ = 2.00 ms, the SMBI valve is closed and no more fuel gas is introduced to the confined plasma volume. The simulation is run until $t$ = 3.00 ms to observe the evolution of the plasma profile.

Figures 2 and 3 illustrate the evolution of the poloidal profile of the plasma density and electron temperature before, during, and after the SMBI. In these figures, the separatrix location is plotted as a dotted line and the limiter is shown at the bottom of each subfigure. Before $t$ = 1.00 ms, the plasma has not yet been fueled by the SMBI, as seen in Figs. 2 (a) and 3 (a). The fuel gas is then launched into the plasma between $t$ = 1.00 - 2.00 ms for a duration of 1.00 ms. As the gas molecules collide with plasma particles, they undergo dissociation and ionization processes. This is evident in the immediate increase in plasma density along the injection path, as shown in Fig. 2 (b). Additionally, Fig. 3 (b) shows that the electron temperature also decreases along the injection path. This is due to the fact that the dissociation and ionization processes require energy from the colliding particles, resulting in a reduction of the ion and electron temperatures. After $t$ = 2.00 ms, the SMBI valve is turned off, however there are still hydrogen molecules and atoms present in the confined volume. These particles continue to dissociate and ionize until they become a plasma. This can be observed in Figs. 2 (e), 2 (f), 3 (e), and 3 (f), where an increase in plasma density and a decrease in temperature can be seen, see also Figs. 2 and 3. Furthermore, we observe that this increase and decrease extends beyond the injection path, which is a result of the diffusion and convection processes of the plasma and fuel particles. As time goes on, the density is gradually distributed throughout the poloidal cross-section of the toka-

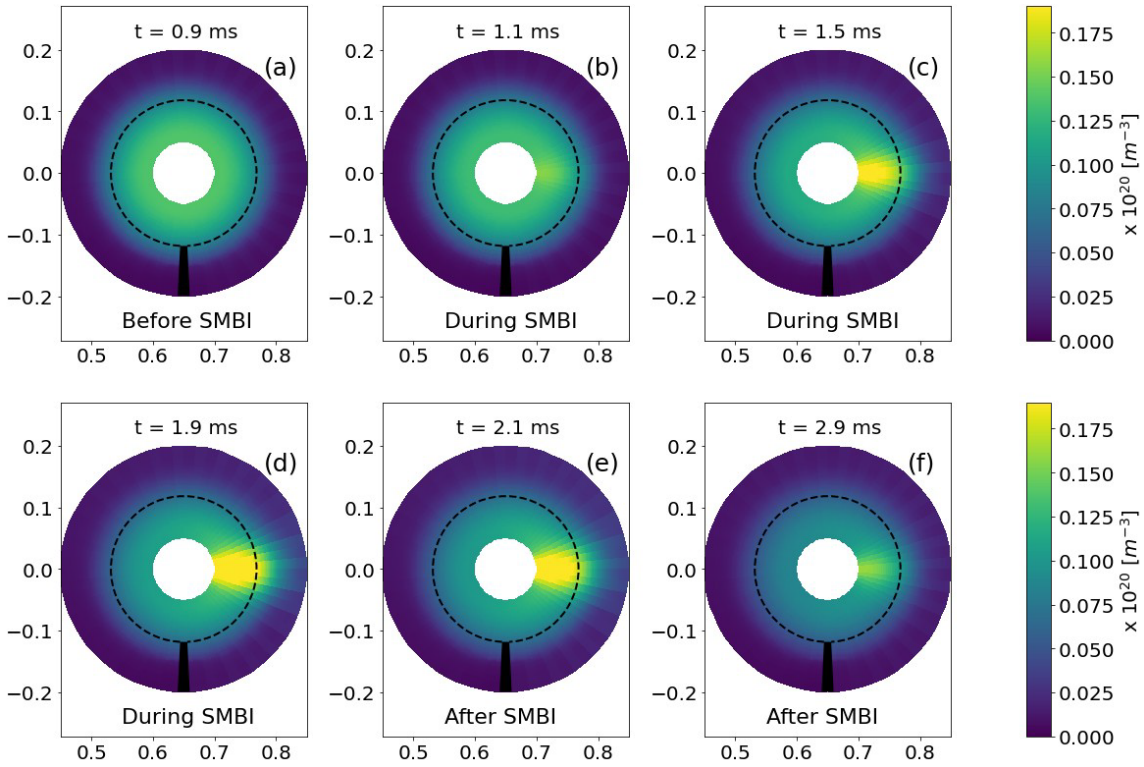


Fig. 2 The change in the plasma density profiles before (a), during (b, c, d), and after the SMBI (e, f) is illustrated. It's worth noting that the gas is introduced to the plasma between $t$ = 1.00 - 2.00 ms. The dotted line represents the separatrix location.

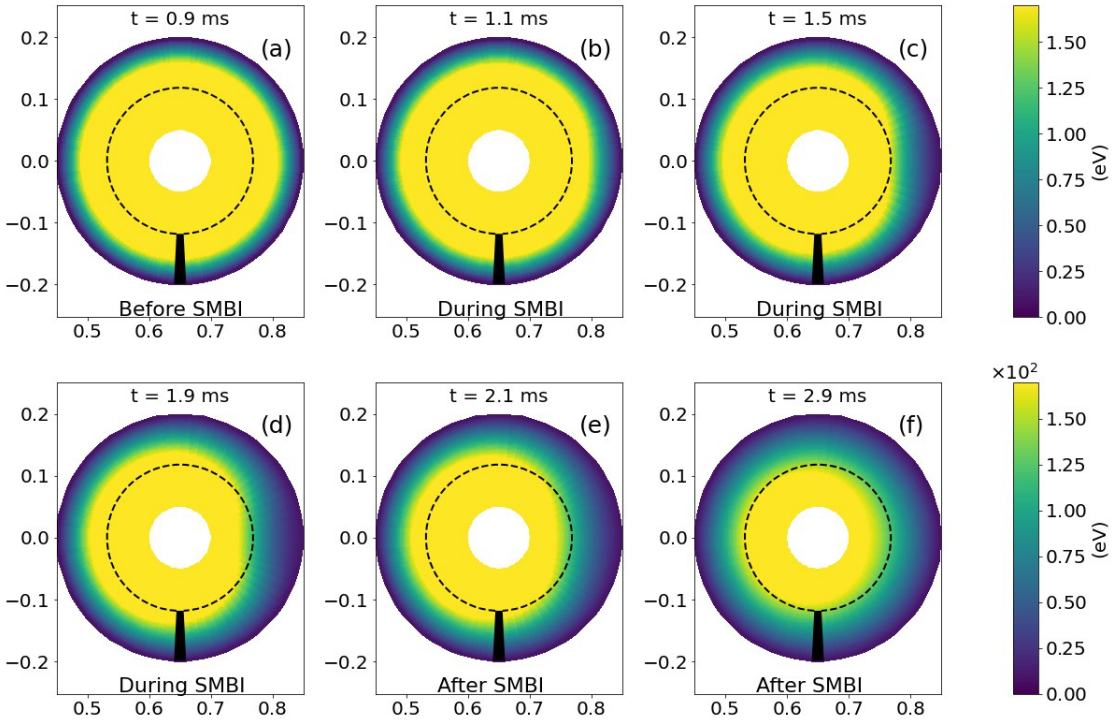


Fig. 3 The illustration shows how the electron temperature profiles change before (a), during (b, c, d), and after the SMBI (e, f). It is important to note that the gas is introduced to the plasma between $t$ = 1.00 - 2.00 ms. The dotted line represents the separatrix location.

mak. We note that large amount of the fuel injection may result in significant drop of temperature, and finally lead to disruption. However, this work does not include the disruption event. The local increase of the density and the drop temperature are temporary. In the future work, one should conduct this analysis.

In Fig. 4, the top row of figure illustrates the radial profiles at several different times along the injection path ($\theta = 3\pi/2$ rad), including (a) the plasma density $n_i$, (b) the atom density $n_a$, (c) the molecule density $n_m$, and (d) the ion temperature $T_i$. The bottom row of figures shows the same quantities as in the top row, but plotted along the poloidal direction at the separatrix ($\psi = 1$). The similar graphs are also plotted in Fig. 5 for the ionization rate $S_i^P$, the dissociation rate $S_{\rm diss}^P$, the radial velocity of molecule gas $V_{\rm xm}$. It is worth noting that the separatrix, which separates the confined plasma from the open field lines, is marked at $\psi = 1$. The limiter is located at the bottom which corresponds to the poloidal angle of $\theta = 0$ rad, and the injection path is at $\theta = 3\pi/2$. Figure 5 (a), the ionization rate near the edge increases after $t$ =1.0 ms due to the increase of the plasma density (Fig. 4 (a)), since the rate is related to the density as follows: $S_i^p = n_e \nu_i = n_a \nu_i^a$.

Initially, the density and temperature profiles exhibit a monotonic increase from the edge to the core, with no fuel molecules or atoms present inside the chamber, as seen in the red lines in Figs. 4 (a) and 4 (c), which correspond to $t = 0.90$ ms. After that, the fuel is delivered along the radial direction at $\theta = 3\pi/2$ rad during $t = 1.00$ - 2.00 ms, mainly due to convection. The molecule density immediately increases, reaching its maximum at the edge, as shown in Figs. 4 (c) and 4 (g). These molecules then dissociate at a rate dependent on the molecule density and the electron temperature, as seen in Figs. 5 (b) and 5 (e). The number density of fuel atoms gradually increases, as evidenced in Figs. 4 (b) and 4 (f). As the atom density increases, the ionization rate also rises. The atoms subsequently turn into plasma through the ionization process, resulting in an increase in the plasma density. This increasing plasma density spreads to other regions through diffusion and convection processes. Furthermore, the injection of the fuel causes a reduction of electron temperature as seen in Figs. 4 (d) and 4 (h).

## 3.2 Simulations with varying injection speeds

The SMBI injection speed greatly influences the penetration depth and efficiency of the fueling process in a tokamak. This section explores the effect of different injection speeds on the plasma state of the tokamak. In order to understand the impact of different injection speeds on the plasma, we compare the radial profiles of several key parameters such as the ion density ($n_i$), electron temperature ($T_e$), ion temperature ($T_i$), molecule density ($n_m$), atom density ($n_a$), and the radial velocity of the fuel molecules ($V_{xm}$) at different injection speeds. Here, we assume that the value of the molecular density at the edge ($n_{m0}$) is $2 \times 10^{17}$ m$^{-3}$, and the SMBI is launched between $t = 1.00$ and 2.00 ms. The data presented in this section were taken at $t = 1.50$ ms, which is 0.50 ms after the start of the fueling.

In Fig. 6, we vary the injection velocity ($V_{xm0}$) over a range of values, from $-600$ m/s to $-1200$ m/s, and observe the resulting changes in the plasma. By comparing

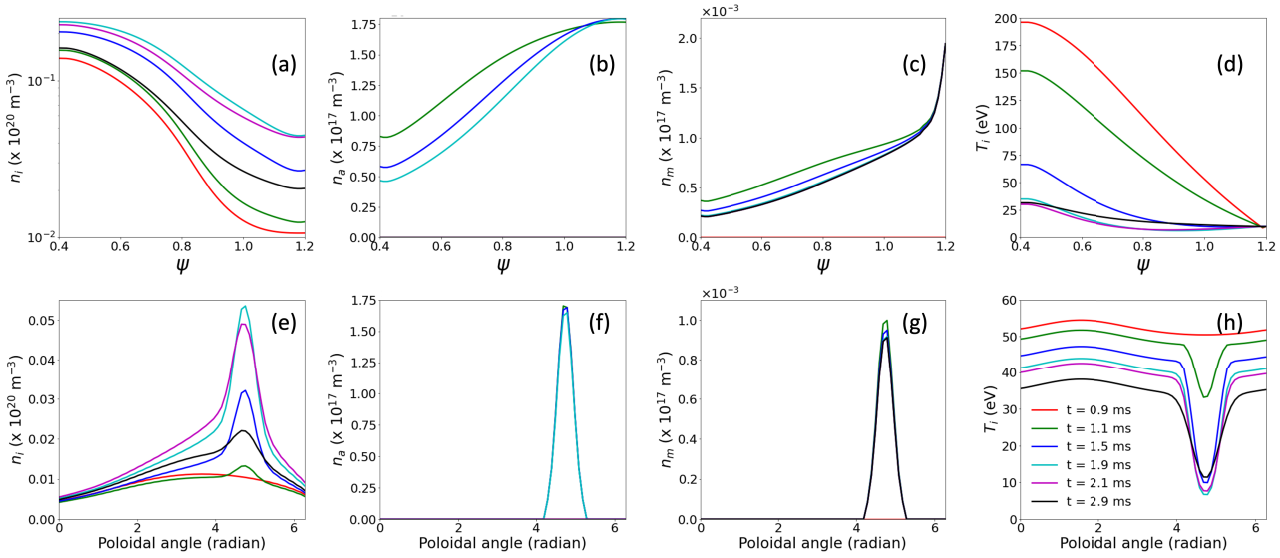


Fig. 4 Top row: the time evolution of radial profiles along the injection path ($\theta = 3\pi/2$ rad), including (a) the plasma density $n_i$, (b) the atom density $n_a$, (c) the molecule density $n_m$, and (d) the ion temperature $T_i$. The separatrix, which separates the confined plasma from the open field lines, is located at $\psi = 1$. Bottom row: the same quantities as in the top row, but plotted along the poloidal direction at the separatrix ($\psi = 1$).

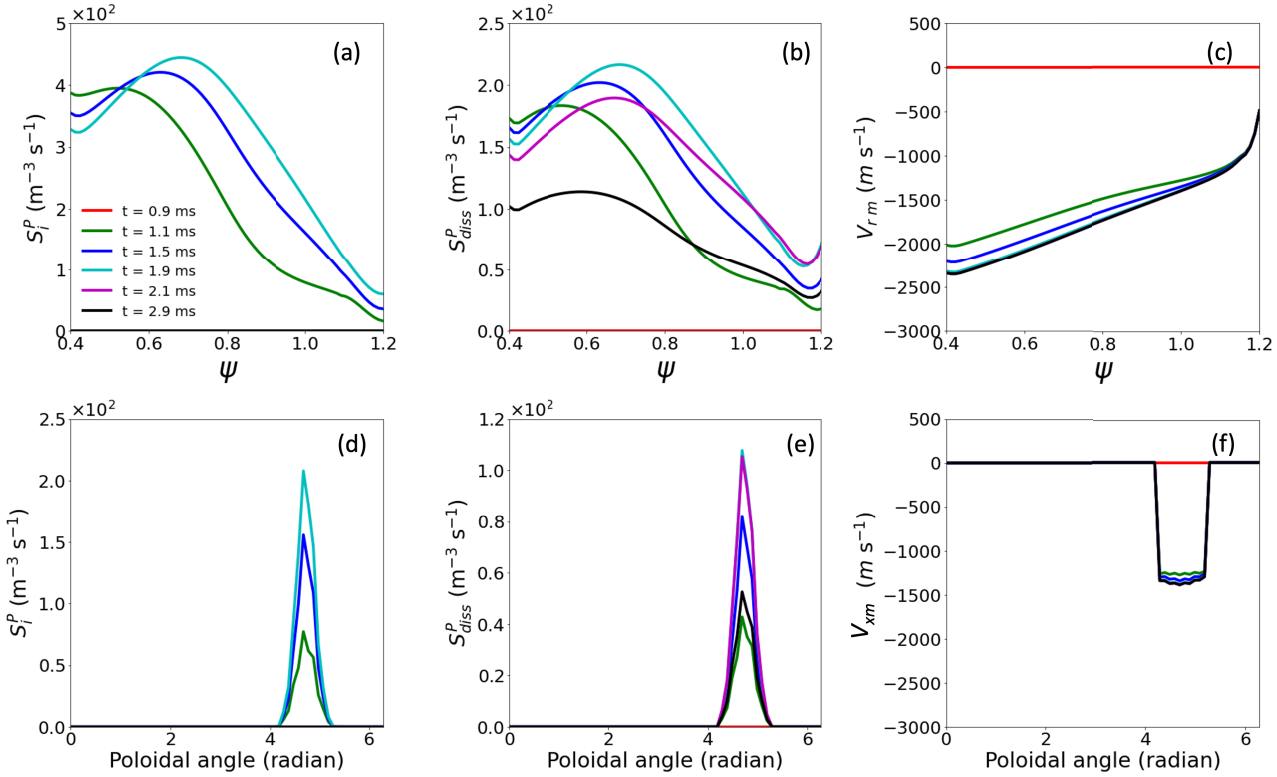


Fig. 5 Top row: the time evolution of radial profiles along the injection path ($\theta = 3\pi/2$ rad), including (a) the ionization rate $S_i^P$, (b) the dissociation rate $S_{\rm diss}^P$, (c) the radial velocity of the fuel molecule $V_{\rm xm}$. Bottom row: the same quantities as in the top row, but plotted along the poloidal direction at the separatrix ($\psi = 1$).

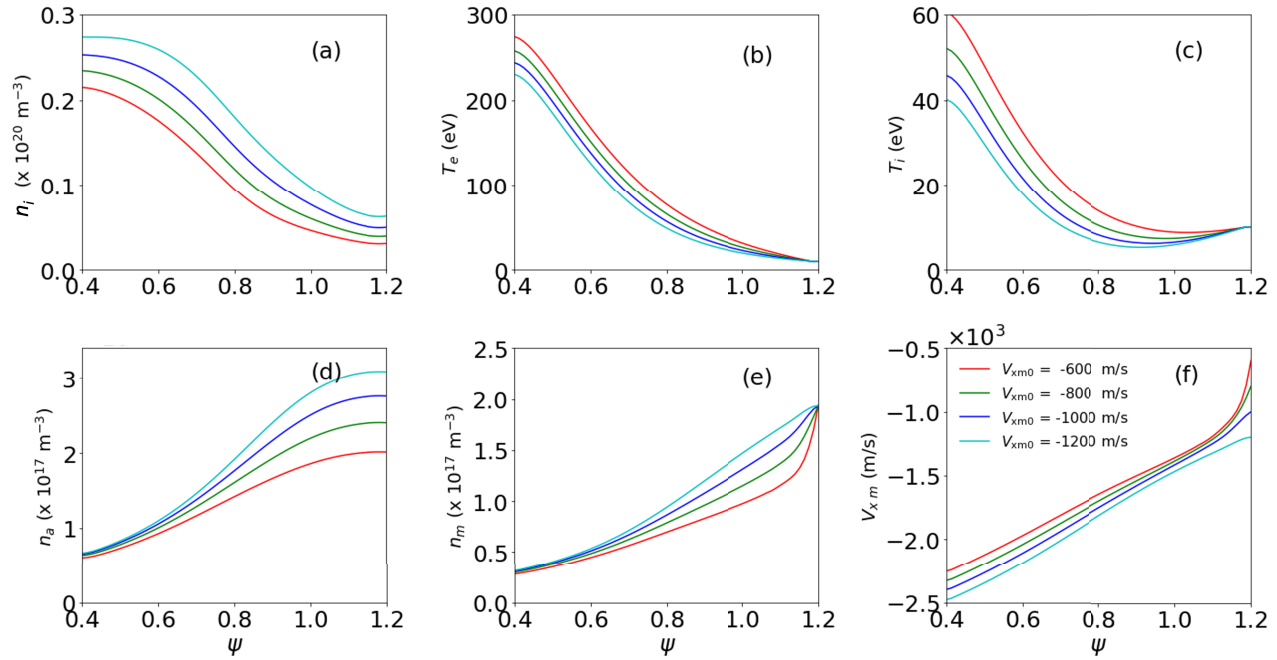


Fig. 6 Comparison of the radial profiles of the ion density ($n_i$), electron temperature ($T_e$), ion temperature ($T_i$), atomic density ($n_a$), molecular density ($n_m$), and the radial velocity of the fuel molecules ($V_{xm}$) at different injection speeds. The data were taken at $t = 1.5$ ms (0.50 ms after the injection).

the radial profiles of various parameters, we can understand how the injection speed affects the penetration depth and efficiency of the fueling process. Increasing the injection speed of the fuel results in a higher molecular influx (see Fig. 6 (e)). This, in turn, leads to higher plasma and atom densities for the increased injection speed. When more molecules and atoms of the fuel gas are present in the inner region, more energy is required for the dissociation and ionization processes. Consequently, this further reduces the electron and ion temperatures, as illustrated in Figs. 6 (b) and 6 (c).

It is noteworthy that the radial speed of the fuel molecule is dominantly influenced by the pressure gradient and the molecular density, as indicated by Eq. (7). At the edge, the speed equals the injection speed of the beam. Subsequently, it experiences a rapid increase at the advancing front of the molecular beam, where the density of molecular particles significantly decreases due to the dissociation of molecules. This reduction in molecular density also results in a decrease in molecular pressure, thereby lowering the radial speed in the inner region, as illustrated in Fig. 6 (f).

The simulation in this section clearly demonstrates that an increased injection speed tends to deliver a greater amount of fuel towards the center. In this part, the molecular density at the edge ($n_{\mathrm{m,edge}}$) is assumed to be $2 \times 10^{17}$ $\mathrm{m}^{-3}$. Assuming a valve radius ($r_{\mathrm{val}}$) of approximately 0.1 mm for producing the supersonic molecular beam and a beam cross-section at the plasma edge ($r_{\mathrm{edge}}$) of about 15 cm, along with the conservation of particles between the valve and the plasma edge and considering the temperature of the fuel to be near room temperature, we can estimate the density at the valve to be $n_{\mathrm{m,val}} = n_{\mathrm{m,edge}} r_{\mathrm{edge}}^2 / r_{\mathrm{val}}^2 \approx 2 \times 10^{24}$ $\mathrm{m}^{-3}$ and the pressure of the beam to be $10^4$ Pa [28]. This should be considered as a minimum level of the beam pressure for the fueling interval of 1.0 ms with an injection speed of 1200 m/s since higher speeds lead to a further drop in temperature, which may terminate the plasma discharge. For a higher beam pressure, the fueling time interval should therefore be reduced.

# 4. Summary

In this study, we use a simulation model based on fluid dynamics to investigate the behavior of the edge plasma of TT-1 during fueling with the SMBI. The simulation is built using the Braginskii equations, which cover various aspects such as the conservation of electron density, the temperatures of ions and electrons, and the momentum of ions and fuel molecules. The equations are outlined in Eqs. (1) to (7). To solve these nonlinear equations, we employed the BOUT++ code, utilizing the finite difference method, in a field-aligned coordinate system that accurately represents the geometry of TT-1 in 2D. It goes beyond traditional 1D simulations by providing a more in-depth examination of plasma and neutral gas interactions in the edge region. Upon fuel injection by the SMBI, the gas quickly interacts with the tokamak plasma, causing the density of fuel molecules to increase near the edge due to convection. As the molecules dissociate, the density of fuel atoms increases and ionizes, resulting in an increase in electron density. This increase can be observed shortly after injection and the electron density spreads throughout the plasma after approximately 10 milliseconds.

Furthermore, we studied the impact of varying the injection speeds of the SMBI between 600 and 1200 m/s on the dynamics of the plasma in the edge region of TT-1. The simulation results suggest that a greater amount of fuel can be delivered into the plasma with an increased injection speed, leading to a reduction in temperature at the edge. We also estimate that, for a fueling time interval of about 1.0 ms, the beam pressure should be approximately $10^4$ Pa with an injection speed of 1200 m/s. The fueling time interval should be reduced if a higher beam pressure is used. The SMBI has been demonstrated as an effective fueling method for long pulse discharges in tokamaks such as EAST [6] and has the potential to mitigate edge-localized modes [10]. In future work, one should also conduct these analysis for TT-1 plasma.

# Acknowledgments

This work was partially funded by the International Atomic Energy Agency (IAEA) through Contract No. 22785. In addition, we would like to express our gratitude for the financial support provided by the Center of Excellence in Theoretical and Computational Science (TaCS-CoE) at KMUTT. This work was also supported by the Thailand Science Research and Innovation (TSRI) Fundamental Fund through project number 4368963. Additionally, this work is part of a collaborative research project under the Center for Plasma and Nuclear Fusion Technology (CPaF).

[1] S. Hong-Juan, D. Xuan-Tong, Y. Liang-Hua, F. Bei-Bin, L. Ze-Tian, D. Xu-Ru and Y. Qing-Wei, Plasma Phys. Control. Fusion **52**(4), 045003 (2010).
[2] J. Xiao, Z. Yang, G. Zhuang, Q. Hu, X. Feng and M. Liu, Plasma Sci. Technol. **16**(1), 17 (2014).
[3] W.W. Xiao, P.H. Diamond, W.C. Kim, L.H. Yao, S.W. Yoon, X.T. Ding, S.H. Hahn, J. Kim, M. Xu, C.Y. Chen *et al.*, Nucl. Fusion **54**(2), 023003 (2014).
[4] H. Takenaga *et al.*, J. Nucl. Mater. **390**, 869 (2009).
[5] X. Zheng, J. Li, J. Hu, J. Li, R. Ding, B. Cao and J. Wu, Plasma Phys. Control. Fusion **55**(11), 115010 (2013).
[6] X. Yuan, J. Li, J. Wu, J. Li, Y. Chen, H. Zhuang, Y. Zhou, X.W. Zheng and J. Hu, Fusion Eng. Des. **134**, 62 (2018).
[7] A. Tamman and N. Somboonkittichai, Plasma Fusion Res. **15**, 2402067 (2020).
[8] D.L. Yu, C.Y. Chen, L.H. Yao, J.Q. Dong, B.B. Feng, Y. Zhou, Z.B. Shi, J. Zhou, X.Y. Han, W.L. Zhong *et al.*, Nucl. Fusion **52**(8), 082001 (2012).
[9] D. Wei, L. Yi, W. Xian-Qu, C. Wei, D. Yun-Bo, S. Ohdachi, J. Xiao-Quan, S. Yong, C. Jian-Yong, Z. Jun *et al.*, Nucl. Fusion **54**(1), 013010 (2013).

[10] W.W. Xiao, P.H. Diamond, X.L. Zou, J.Q. Dong, X.T. Ding, L.H. Yao, B.B. Feng, C.Y. Chen, W.L. Zhong, M. Xu *et al*., Nucl. Fusion **52**(11), 114027 (2012).
[11] R. Schneider, X. Bonnin, K. Borrass, D.P. Coster, H. Kastelewicz, D. Reiter, V.A. Rozhansky and B.J. Braams, Contrib. Plasma Phys. **46**(1-2), 3 (2006).
[12] E.L. Vold, F. Najmabadi and R.W. Conn, Nucl. Fusion **32**(8), 1433 (1992).
[13] T.D. Rognlien, B.J. Braams and D.A. Knoll, Contrib. Plasma Phys. **36**(2-3), 105 (1996).
[14] T.D. Rognlien, D.D. Ryutov, N. Mattor and G.D. Porter, Phys. Plasmas **6**(5), 1851 (1999).
[15] Y.-H. Wang, W.-F. Guo, Z.-H. Wang, Q.-L. Ren, A.-P. Sun, M. Xu, A.-K. Wang and N. Xiang, Chinese Physics B **25**(10), 106601 (2016).
[16] J. Promping, A. Wisitsorasak, B. Chatthong and K. Nilgumhang, Plasma Fusion Res. **15**, 2403033 (2020).
[17] S.I. Braginskii, Sov. Phys. JETP **6**(33), 358 (1958).
[18] Z.H. Wang, X.Q. Xu, T.Y. Xia and T.D. Rognlien, Nucl. Fusion **54**(4), 043019 (2014).
[19] B.D. Dudson, M.V. Umansky, X.Q. Xu, P.B. Snyder and H.R. Wilson, Comput. Phys. Commun. **180**(9), 1467 (2009).
[20] B.D. Dudson, A. Allen, G. Breyiannis, E. Brugger, J. Buchanan, L. Easy, S. Farley, I. Joseph, M. Kim, A.D. McGann *et al.*, J. Plasma Phys. **81**(1), (2015).
[21] T.Y. Xia, X.Q. Xu and P.W. Xi, Nucl. Fusion **53**(7), 073009 (2013).
[22] M.A. Beer, S.C. Cowley and G.W. Hammett, Phys. Plasmas **2**(7), 2687 (1995).
[23] F. Hariri and M. Ottaviani, Comput. Phys. Commun. **184**(11), 2419 (2013).
[24] J. Promping, S. Sangaroon, A. Wisitsorasak, B. Chatthong, R. Picha and T. Onjun, Plasma Fusion Res. **13**, 3403094 (2018).
[25] M.J. Seaton, Monthly Notices of the Royal Astronomical Society **119**(2), 81 (1959).
[26] G.-S. Jiang and C.-W. Shu, J. Comput. Phys. **126**(1), 202 (1996).
[27] S. Buaruk, T. Makmool, J. Promping, T. Onjun, S. Sangaroon, A. Wisitsorasak, J. Garcia and B. Chatthong, Plasma Fusion Res. **14**, 3403153 (2019).
[28] G.L. Xiao, W.L. Zhong, X.R. Duan, B.B. Feng, C.Y. Chen, J. Bucalossi, X.L. Zou, J.S. Hu, J.-G. Kwak, W.W. Xiao *et al*., Reviews of Modern Plasma Physics **7**(1), 2 (2022).